Taguchi method: artificial neural network approach for the optimization of high-efficiency microfluidic biosensor for COVID-19

Imed Ben Romdhane[1], Asma Jemmali[1], Sameh Kaziz[2,3], Fraj Echouchene[1,4], Thamraa Alshahrani[5,a], Hafedh Belmabrouk[1,6,b]

[1] Laboratory of Electronics and Microelectronics, Faculty of Science of Monastir, University of Monastir, 5019 Monastir, Tunisia
[2] Quantum and Statistical Physics Laboratory, Faculty of Sciences of Monastir, University of Monastir, 5019 Monastir, Tunisia
[3] Higher National Engineering School of Tunis, Taha Hussein Montfleury Boulevard, University of Tunis, 1008 Tunis, Tunisia
[4] Higher Institute of Applied Sciences and Technology of Sousse, Sousse, Tunisia
[5] Department of Physics, College of Science, Princess Nourah Bint Abdulrahman University, Riyadh, Saudi Arabia
[6] Department of Physics, College of Science, Majmaah University, Al Majma'ah 11952, Saudi Arabia

Abstract COVID-19 is a pandemic disease caused by severe acute respiratory syndrome coronavirus 2 (SARS-CoV-2). This virus is mainly spread by droplets, respiratory secretions, and direct contact. Caused by the huge spread of the COVID-19 epidemic, research is focused on the study of biosensors as it presents a rapid solution for reducing incidents and fatality rates. In this paper, a microchip flow confinement method for the rapid transport of small sample volumes to sensor surfaces is optimized in terms of the confinement coefficient β, the position of the confinement flow X, and its inclination α relative to the main channel. A numerical simulation based on two-dimensional Navier–Stokes equations has been used. Taguchi's $L_9(3^3)$ orthogonal array was adopted to design the numerical assays taking into account the confining flow parameters (α, β, and X) on the response time of microfluidic biosensors. Analyzing the signal-to-noise ratio allowed us to determine the most effective combinations of control parameters for reducing the response time. The contribution of the control factors to the detection time was determined via analysis of variance (ANOVA). Numerical predictive models using multiple linear regression (MLR) and an artificial neural network (ANN) were developed to accurately predict microfluidic biosensor response time. This study concludes that the best combination of control factors is $\alpha_3\beta_3X_2$ that corresponds to $\alpha = 90°$, $\beta = 25$ and $X = 40\,\mu$m. Analysis of variance (ANOVA) shows that the position of the confinement channel (62% contribution) is the factor most responsible for the reduction in response time. Based on the correlation coefficient (R^2), and value adjustment factor (VAF), the ANN model performed better than the MLR model in terms of prediction accuracy.

1 Introduction

The Covid-19 pandemic is an emerging infectious disease, which causes high mortality and affects the economy and health system [1, 2]. This virus presents as a severe acute respiratory syndrome [3]. Infection with this virus appears in initial symptoms, such as fever, cough, muscle aches, or feeling very tired, and some cases may progress to pneumonia and acute respiratory illnesses, especially in the older and people with chronic diseases [4]. To achieve an effective solution than inventing a new vaccine, the rapid detection of this virus seems to be a faster and less expensive solution [5]. For this purpose, the study of a biosensor has attracted attention, recently to control the pandemic situation [6]. Among these biosensors are microfluidic devices that can be adopted to quantify antibodies and protein biomarkers with accuracy and relative ease compared to traditional methods. Microfluidic biosensors are devices that can detect the presence or activity of biological molecules in samples, such as blood [7], urine[8], saliva [9] or water [10]. They are increasingly used in the fields of biology [11], the environment [12], food safety [13] and medicine [11, 14]. Microfluidic biosensors are increasingly used for the detection of infectious diseases, including COVID-19 [15, 16]. Antibodies to SARS-CoV-2 can be detected with ease, reliability, and cost-effectiveness using these devices. Seo et al. [17] have developed a biosensor device based on a field effect transistor for the detection of SARS-CoV-2 in clinical samples. The device has successfully detected the virus in a culture medium for a specific concentration. In another report, Layqah et al. [18] have developed an electrochemical immunosensor for the detection of MERS-CoV. The detection is performed on a gold nanoparticle-modified carbon electrode with square wave voltammetry. Using bioactivated microchannels and antibody-functionalized microspheres, Javanmard [19] developed a label-free impedance-based protein biomarker sensor. As low as 1 ng/ml concentration of anti-hCG antibodies could be detected

with the researchers' system after one hour of assaying. An IgG antibody quantification device developed by Dong et al. [20] uses a screen-printed microfluidic device. With this device, the detection limit is approximately 10 ng/mL, and the dynamic range is 100 ng/ml to 10 ug/ml. Chin et al. [21] developed a miniaturized ELISA microfluidic chip named mChip (Mobile Microfluidic Chip for Protein Biomarker Immunoassay) using a small amount (< 1 µL) of untreated whole blood. An immunoassay-based multiplexed microfluidic device by Lafleur et al. [22] detected disease-specific antigens or IgM antibodies in blood via a disposable microfluidic device. An ELISA test at benchtop level can detect 20 ng/ml in 30 min. Lee et al. [23] developed an integrated microfluidic sensor for the detection of dengue virus IgG and IgM antibodies in human serum. The detection limit is 21 pg and the total assay time is approximately 30 min. Surface plasmon resonance (SPR) sensor, impedance-based sensor and immunoassays are the main methods used in most cases for the detection of biomolecules. These sensors involve the same specific binding kinetics of analytes and immobilized ligands. They mix a small concentration of a biological analyte with the fluid in a microchannel. When the analyte takes longer to be transported by convection and diffusion to the sensitive surface than the chemical reaction, the entire reaction is retained by the mass transport process usually causing the formation of a diffusion boundary layer [24]. This leads to the limitation of the response time and performance of the microfluidic biosensor. In order to improve the reaction rate, several experimental and numerical approaches have been developed [25–35]. Selmi et al. [28, 36] have analyzed the electrothermal effect on the immunoassay of a biosensor. They studied the binding reaction efficiency in the microchannel of a biosensor with asymmetrical interdigitated electrodes. In another study, Selmi et al. [28] have analyzed the effect of the cylindrical obstacle on the microfluidic biosensor efficiency. On the other hand, Selmi et al. [29] studied the effect of confinement by the secondary flow on the chemical kinetics but they did not optimize the confinement parameters. Echouchene et al. [30] have improved the analyte transport of microfluidic immunosensors using a new sensing area shape. In a recent study, Kaziz et al. [31] optimized the design parameters of an electrothermal flow biosensor for SARS-CoV-2 protein *S* immunoassay. Recently, Kaziz et al. [31, 32] have developed numerical methods for optimizing the performance of microfluidic biosensors for the detection of COVID-19. Based on the Taguchi method, they determined the degree of influence of different optimization parameters [32]. In a very recent work, Kaziz et al. [33] and Ben mariem et al. [34] used the Taguchi approach and artificial intelligence based on artificial neural networks for the optimization of the performance of a microfluidic biosensor under electrothermal force for the detection of COVID-19. Excellent results were obtained in this work.

In this work, we propose the optimization of a two-dimensional configuration to confine an analyte flow to the surface of the microfluidic biosensor. Two-dimensional Navier–Stokes equations coupled with the analyte transport and binding reaction equations are used for this simulation. The effects of confinement flow parameters such as the confinement flow coefficient, the position of the confinement channel and its angle with respect to the main channel are analyzed by calculating the response time via the time evolution of the average concentration of the complex analyte-ligand. This paper follows the following plan: In Sect. 2, we describe the mathematical model describing our physical problem as well as the geometric configuration studied. The numerical method has been described in this section. Section 3 is devoted to the presentation of the results of the numerical calculation of the effect of the optimization parameters. In this section, we have presented the different configurations to be analyzed. An experimental design approach based on the Taguchi method was used in this section to give the best combination of the studied factors as well as their contribution percentages in the response time of the microfluidic biosensor with confinement. Finally, two models, one based on multiple linear regression (MLR) and the other on artificial neural network (ANN), were developed to predict the biosensor response time.

2 Physical model and boundary conditions

2.1 Geometric structure

The modeled system involves mixing a small concentration of a biological analyte with the water in a microchannel where a reaction surface is located on the bottom wall of the microchannel. A secondary water flow (inlet 2) without an analyte located on the top with an angle of inclination α to the primary flow (inlet 1). The analyte flows through a microfluidic channel of dimensions $40 \, \mu m \times 40 \, \mu m \times 250 \, \mu m$. Figure 1 shows the three-dimensional structure of a microfluidic biosensor suitable for the detection of COVID-19.

2.2 Physical model

The proposed work is based on the two-dimensional Navier–Stokes equations for the numerical simulation of the fluid flow inside the microchannel. For this purpose, the fluid is assumed to be incompressible so that [37]:
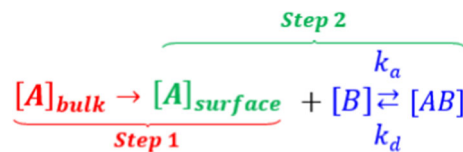
$$\nabla . \overrightarrow{U} = 0 \tag{1}$$

$$\rho \nabla \left(\overrightarrow{U} \otimes \overrightarrow{U} \right) - \mu \nabla^2 \overrightarrow{U} + \nabla p = 0 \tag{2}$$

where $\overrightarrow{U}$ is the velocity vector, ρ is the density, μ is dynamic viscosity, and p is the pressure.

Fig. 1 Tridimensionnel configuration of the microfluidic biosensor with confinement flow
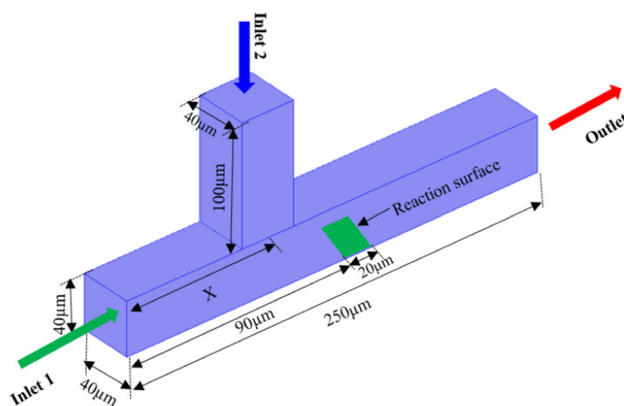
Fig. 2 Kinetic reaction process

Table 1 Boundary conditions used for the simulation

Type	Navier–stokes equations	Analyte transport
Inlet 1	Average inlet velocity u_{ave}	Concentration $C = C_0$
Inlet 2	Average inlet velocity $u_2 = \beta \times u_{ave}$	Convectif flux: $\vec{n}.\left(-D\vec{\nabla}C\right) = 0$
Outlet	$\left(\frac{\partial U}{\partial x}\right)_{L,y} = 0$	$\left(\frac{\partial [C]}{\partial x}\right)_{t,L,y} = 0$
Wall	No-slip velocity	$\frac{\partial C}{\partial n} = 0$
Reaction surface	No-slip velocity	$-\vec{n}.\left(-D\vec{\nabla}C + C\vec{U}\right) = \frac{\partial [AB]}{\partial t}$

The detection of these sensors is based on the immobilized analytes and ligands. The immunosensors are the necessary tools for the detection of analytes in antibody-antigen interactions [38–41]. The reaction surface of a biosensor is a liquid–solid surface in which specific recognition of immobilized analytes and ligands occurs. The kinetics of the reaction takes place in two steps [42] (Fig. 2):

- Step 1: diffusion of analyte from bulk to the reaction surface.
- Step 2: binding reaction between the analyte and the ligands.

where $[A]_{bulk}$ and $[A]_{surface}$ are the analyte concentration in the bulk and at the reaction surface, respectively. $[B]$ stands for the ligand concentration and $[AB]$ is the complex concentration, k_a and k_d are respectively the association and dissociation rates.

The transient analyte transport of biological species is described by Fick's second law:

$$\frac{\partial [C]}{\partial t} + \overrightarrow{U}.\nabla[C] = D\nabla^2[C] \tag{3}$$

where $[C]$ is the analyte concentration and D is the diffusion coefficient of the analyte.

Using the first-order Langmuir adsorption model, the reaction rate at the reaction surface between ligand and analyte is:

$$\frac{\partial [AB]}{\partial t} = k_a[A]_{surface}\left\{[B_0] - [AB]\right\} - k_d[AB] \tag{4}$$

where $[B_0]$ is the ligand density.

2.3 Boundary conditions

In order to solve the previous system of equations, boundary conditions must be applied. Table 1 summarizes the boundary conditions used for this simulation.

2.4 Numerical method

The finite element method was used to solve the mathematical model of this problem [28]. The equations from 1 to 4 are solved by the finite element method [28], which consists in seeking an approximate solution after discretization of the domain into triangular

Table 2 Input parameters used for model validation

Parameters	Value(s)
Input analyte concentration c_0	10 (μmol/m^3)
Analyte diffusion coefficient D	3×10^{-11} m^2/s
Antibody ligand concentration $[B_0]$	2.387×10^{-7} mol/m^2
Dissociation rate k_d	3.5×10^{-3} s^{-1}
Association rate k_a	240 m^3/mol s
Diameter of reaction surface	4 mm
Inlet flow Q_v	66 μL/min

Fig. 3 Validation of numerical results of the normalized complex concentration with the experimental data of Hofmann et al. [25] for flow rate Qv = 66 μL/min
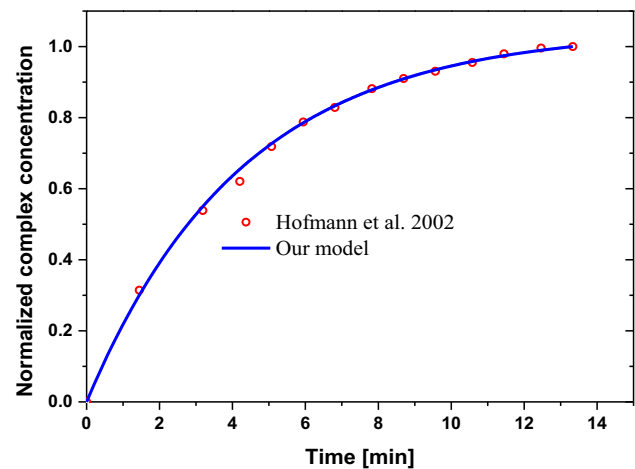
elements refined in the vicinity of the reaction surface whose concentration gradient is significant. By applying the weak formulation, Eqs. (1)–(4) are transformed into a non-dependent and time-dependent system of ordinary equations. The temporal discretization of the ordinary differential equations was carried out via the explicit Euler method. Newton's method was adopted for solving the problem. After the spatial discretization of the field of study, we adopted the following approach to solve the differential problem: In the first case, we solve the Navier–Stokes equations to determine the velocity field then we simultaneously solve the analyte transport equation coupled with the equation of transient chemical kinetics to determine the concentrations of the target analytes, $[C]$ in the microchannel and the concentration of the analyte/ligand complex $[AB]$ on the sensitive surface.

3 Results and discussion

3.1 Validation

First, the physical model is validated against results taken from the literature [25]. The data used for validation is shown in the following Table 2 for a 3D configuration of dimension 25 mm × 5 mm × 0.02 mm.

Figure 3 shows that obtained results with the current numerical study are in good agreement with the experimental data of Hofmann et al. [25].

3.2 3D to 2D approximation

Assuming that the variation in analyte concentration is small along the y-axis, the 3D geometry can be reduced to a 2D approximation [25]. Figure 4 shows that a good agreement is obtained for 2D results compared to 3D simulation. Thus, the two-dimensional microfluidic biosensor will be considered, hereafter, in order to study the effect of several physical and geometrical parameters on the performance of microfluidic biosensors.

3.3 Design of microfluidic biosensor

Three microfluidic biosensors with different angles $\alpha = 30°, 60°,$ and $90°$ were used to improve the time detection of the COVID-19 virus. Each inlet was set to 40 μm high, and 100 μm length. The sensor, 20 μm wide, is placed on the bottom wall, 90 μm from inlet 1. The detailed diagram of the four configurations of microfluidic biosensors is shown in Fig. 5.

Fig. 4 Validation of 3D/2D approximation
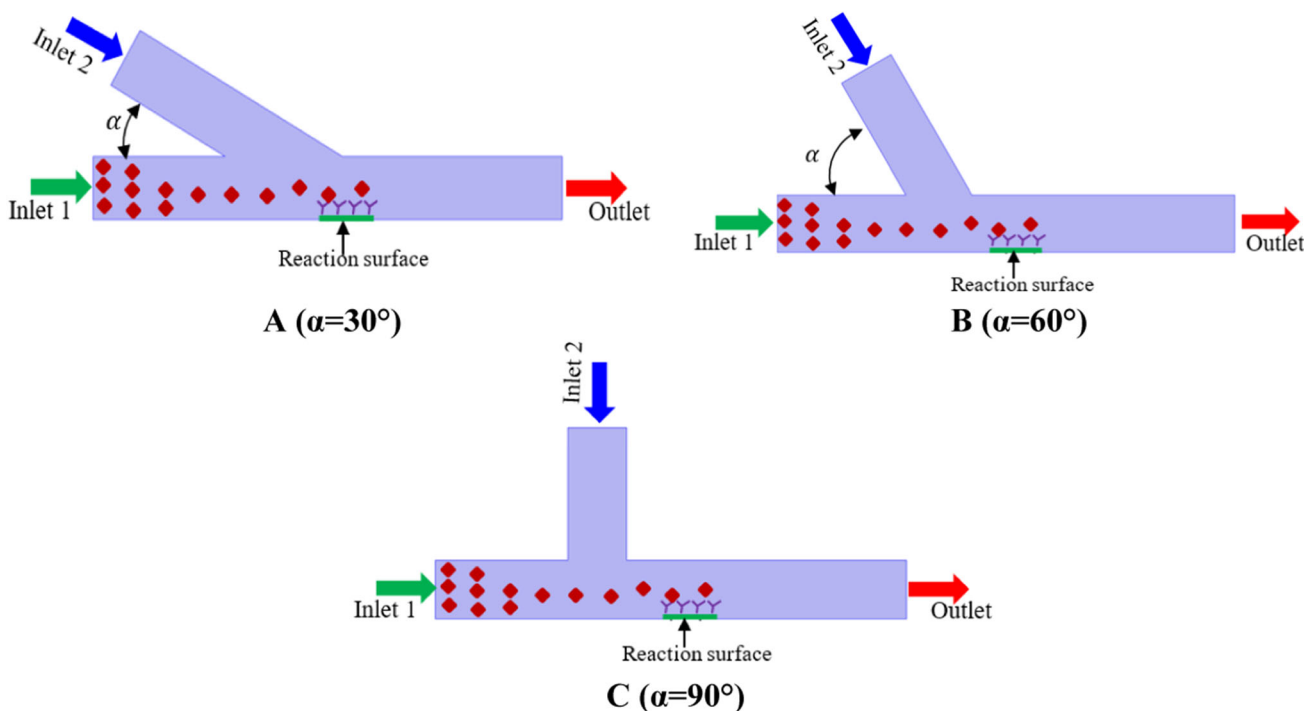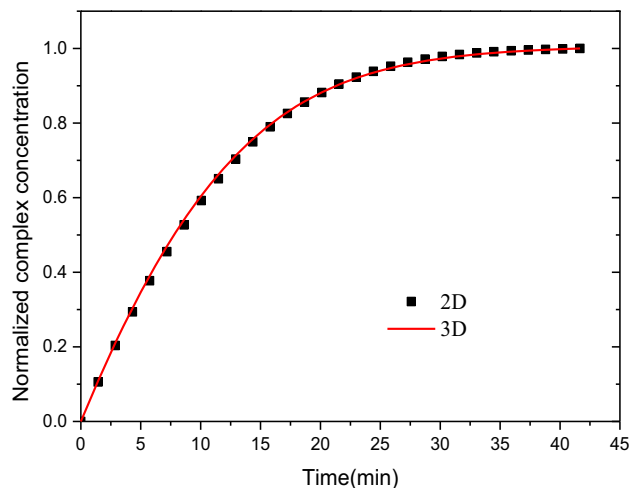
Fig. 5 Schematic diagram of four microfluidic biosensors for different angles between inlets **A** $\alpha = 30°$, **B** $\alpha = 60°$ and **C** $\alpha = 90°$. All proposed configurations are 250 µm in length and have a cross section of 40 µm width and 40 µm height

For an electrochemical problem, the convective diffusion equation was solved by Levich et al. [43, 44] and given as:

$$k_m = 0.98 D^{\frac{2}{3}} \left(\frac{u}{h \times l} \right)^{1/3} \tag{5}$$

where D is the analyte diffusion coefficient, u is the average inlet velocity, h is the channel height and l is the position along the sensing zone. The thickness of the diffusion layer, for $[A] < [A_0]$, can be calculated as:

$$d_{\text{diff}} = \frac{D}{k_m} = \frac{1}{0.98} \left(\frac{D \times h \times l}{u} \right)^{1/3} \tag{6}$$

The affinity of the antibodies used for the detection of SARS-COV is 10^6 Mol/m^3 [45] and the absorption and dissociation rates are 10^3 m^3/Mol s and 10^{-3} s^{-1} respectively. In the numerical simulation, sample analyte concentration flows a 250 µm microchannel length. A reaction surface of 20 µm in length with a ligand concentration of 1.668×10^{-8} mol/m^2 is used. The diffusion coefficient of the analyte is 3×10^{-11} m^2/s. The association and the dissociation rates are 7.5 m^3/mol s and 6.6×10^{-4} s^{-1}, respectively.

Table 3 Levels of each factor in this study

Symbol	Optimization parameter	Level 1	Level 2	Level 3
A	Inclination angle α (°)	30	60	90
B	Confinement coefficient β	5	10	25
C	Confinement position X (μm)	0	40	80

Table 4 Experimental configurations for the response time according to the $L_9\left(3^3\right)$ factorial design

Configuration test	α	β	X
1	30	5	0
2	30	10	40
3	30	25	80
4	60	5	40
5	60	10	80
6	60	25	0
7	90	5	80
8	90	10	0
9	90	25	40

3.4 Optimization with the Taguchi method

3.4.1 Taguchi method

The Taguchi method is a robust technique for the optimization of multivariate systems, including mass transport in microfluidic biosensors, where response time is controlled by several key factors with an optimization goal. The Taguchi method involves optimizing key factors to achieve the desired goal with the application of mathematical and statistical concepts. This method is used in this study to minimize the microfluidic biosensor response time. Taguchi method uses the orthogonal array (OA) networks that form the matrix of numerical experiments and the signal-to-noise ratio (S/N) to study a large number of variable processes with a small number of numerical experiments.

3.4.2 Factors and levels

For the optimization of two-dimensional microfluidic confinement for microfluidic biosensors for the detection of COVID-19, the Taguchi method was used in order to evaluate the influence of the chosen independent variables which are the inclination angle α, the confinement coefficient β, and confinement position X. The factors and levels used in the present study are summarized in Table 3. These factors are selected based on the above numerical database. In this study, the response time T_R is taken as the signal factor.

3.4.3 Taguchi approach

Taguchi's method is an approach for modeling difficult multivariate systems where the response is pretentious from several key factors with an optimization goal. This approach involves optimizing key parameters to achieve the desired goal with applications of mathematical and statistical concepts. This method is used in this work to minimize the microfluidic biosensor response time with confinement. Rather than using a large number of numerical experiments to study a large number of variables, Taguchi used orthogonal (OA) matrices to study a large number of variables [33].

Through OA, maximum information can be obtained in a minimum number of numerical experiments and optimal levels can be determined for each parameter.

In the present study, the L_9 orthogonal matrix is chosen based on the number of key factors and their levels. With Taguchi fractional factorial design, there are only nine experiments required instead of 27 for three factors at three levels in a factorial design. In the Taguchi method, the least number of executions possible can be estimated as follows [46]:

$$N_{\text{Taguchi}} = 1 + \text{NF}(L - 1) \tag{7}$$

where N_{Taguchi} is the minimum number of experiments to perform, NF is the number of control factors and L is the number of levels used. In the present study, three parameters (NF = 3) and three levels ($L = 3$) were considered as shown in Table 3. Using this equation, a minimum of 7 numerical experiments are required. However, for three level factors, only the L_9 orthogonal array is available. Table 4 shows the three parameter levels for each run using the orthogonal array closest to L_9 for the present experimental runs.
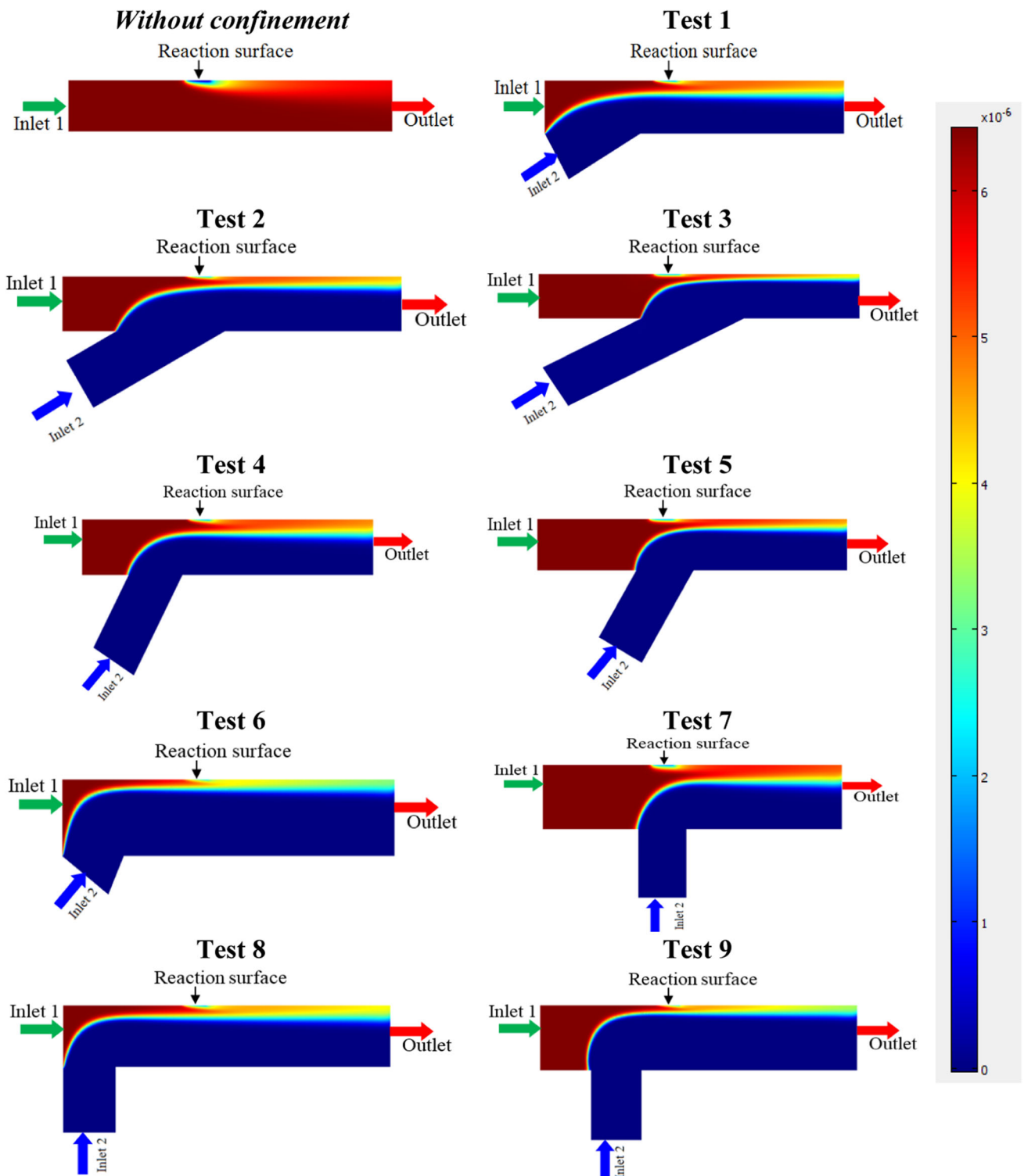
Fig. 6 The development of the diffusion boundary layer of the binding reaction. (1) without confinement and (2–9) for configurations of Table 4 at time of 150 s

Figure 6 shows the analyte diffusion boundary layers during the association phase for all the assays in Table 5 at $t = 150$ s compared with that without confinement. The boundary layer gradually disappears in the association phase because the confinement coefficient is so important when the confinement channel is in front of the reaction surface.

Figure 7 illustrates the response of microfluidic biosensor for all experiment configurations that are enumerated in Table 4. The curves are plotted as the average surface concentration of complexes versus time.

Table 5 Results of the L_9 experimental configurations

Experiment	Response time T_R (min)	S/N ratio (dB)
1	5.37	− 14.5995
2	4.9	− 13.8039
3	6.2	− 15.8478
4	5.3	− 14.4855
5	6.01	− 15.5775
6	4.16	− 12.3819
7	6.53	− 16.2983
8	4.81	− 13.6429
9	3.71	− 11.3875

Fig. 7 Complex concentration in association phase for all tests illustrated in Table 4
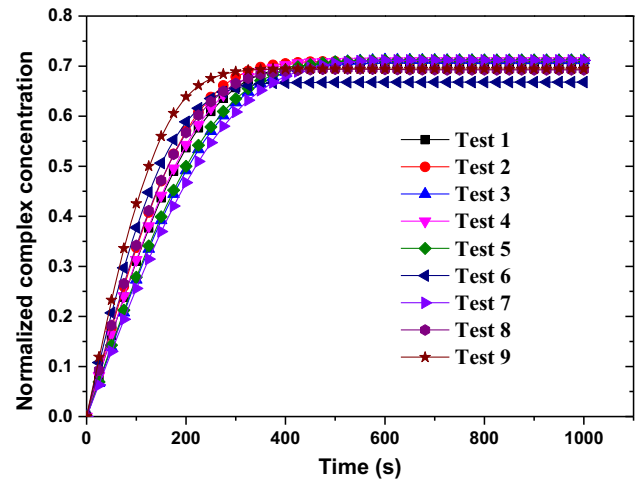
3.4.4 Signal-to-noise analysis

The signal-to-noise ratio, introduced by Taguchi, is used in quality engineering and experimental design. It can help engineers determine the effectiveness of control factor levels. The S/N ratio makes it possible to obtain the optimal parameters of these responses. Since the lowest value of the response time is a desirable condition to achieve a higher performance of the microfluidic biosensor, the best S/N ratio approach has been adopted to schematize the S/N ratio. The characteristic "smaller is better" means that the smaller the value of an objective function f, the closer the systematic optimization of the control factors is [32]:

$$S/N = -10 \log \left(\frac{1}{n} \sum_{i=1}^{n} y_i^2 \right) \tag{8}$$

where n is the total number of simulation tests and y_i is the calculated response time value at a given factor combination.

3.4.5 Evaluation of numerical results

Table 5 shows the L_9 orthogonal array of the three control factors, detection times, and signal-to-noise ratios (SNRs) calculated for each experimental configuration. The detection time is the time during which the average concentration is equal to 95% of its saturation value [32].

The factorial effect and contribution ratio of every factor are presented in Table 6 and Fig. 8a and b, respectively. To assess the effect of each key parameter, the mean values of the responses time and S/N ratio obtained for each level must be calculated. To do this, the sum of the results associated with each level of the orthogonal table divided by the number of tests for this level provides the appropriate averages which is equal to 5.22 min for T_R and− 14.22 dB for S/N ratio. The S/N ratio response table for T_R is shown in Table 5. Using Tables 4 and 5, it is straightwordward to obtain the results summarized in Table 6. This table indicates the optimal levels of the simulation variables responsible for the minimum T_R which are also graphically represented in Fig. 8a and b.

The optimal combination of control factors for minimum response time T_R of microfluidic biosensor for COVID-19 can be easily detected either from Table 6 or from Fig. 8a and b. The optimization factor levels giving the minimum response time T_R have been specified by bold numbers in Table 6 and surrounded with a circle in Fig. 8a and b. The horizontal magenta line indicates the average value over all the configurations. For the inclination angle α, the optimal level is level 3 (mean = 5.017 and S/N ratio =

Table 6 Average peak-to-peak value of response time and S/N ratio for all levels of all factors

Level	Response time T_R			S/N ratio		
	α	β	X	α	β	X
1	5.490	5.733	4.780	− 14.75	− 15.13	− 13.54
2	5.157	5.240	**4.637**	− 14.15	− 14.34	**− 13.23**
3	**5.017**	**4.690**	6.247	**− 13.78**	**− 13.21**	− 15.91
Delta	0.473	1.043	1.610	0.97	1.92	2.68
Rank	3	2	1	3	2	1

The values written in bold designate the optimal level for the variable. The value of delta corresponds to difference between the maximal value and the minimal value

Fig. 8 mean of **a** response time TR and **b** S/N ratio for the three key parameters at different levels
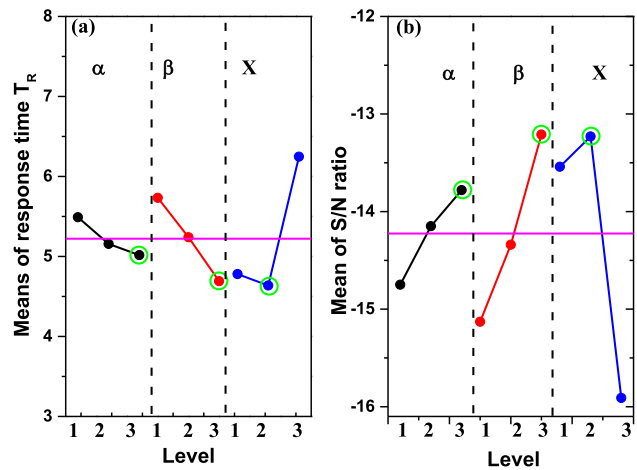
Fig. 9 Pareto chart of the standardized effects of response time for confidence level 95%
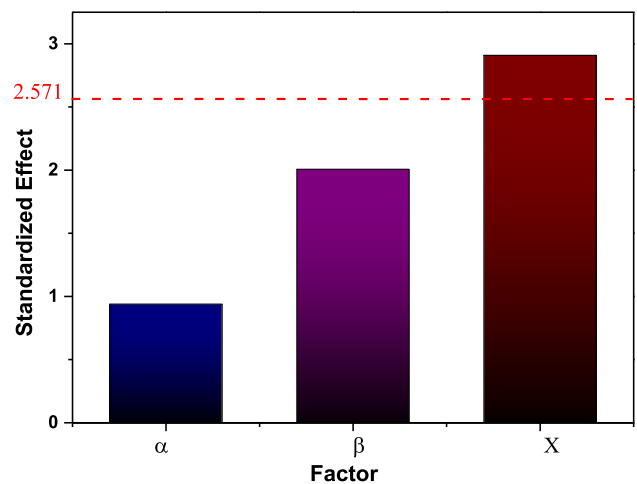
− 13.78 dB). In regards to the confinement coefficient β, the optimal level is level 3 (mean = 4.69 and S/N ratio = − 13.21 dB). Finally, the optimal level of the confinement channel position X is obtained for level 2 (mean = 4.637 and S/N ratio = − 13.23 dB). Especially, the minimum response time was achieved with the following papameters: $\alpha_3 \beta_3 X_2$ that corresponds to $\alpha = 90°$, $\beta = 25$ and $X = 40\,\mu\text{m}$.

The factor with the strongest influence was determined by the difference values, Delta, between the maximum value and the minimum value of the average values obtained (Table 6). The greater the difference, the more influential the control factor. Figure 8a and b and Table 6 indicate that the value of Delta related to the parameter X is greater that the two other values of delta related to the angle α and the confinement coefficient. Therefore, the confinemnt channel position X has the strongest influence.

In order to determine the magnitude and significance of the effects of three optimization factors, the Pareto chart is used (Fig. 9). Figure 9 shows the absolute values of the standardized effects from largest effect to smallest effect. Only the X factor intersects the reference line at 2.571 which shows that it is statistically significant at the 0.05 level.

Table 7 ANOVA results for response time

Optimization parameter	DoF	SS	F	P	% Contribution
Inclination angle α	2	1.4501	1.47	0.405	6.93
Confinement coefficient β	2	5.6023	5.67	0.150	26.76
Confinement position X (μm)	2	12.8941	13.05	0.071	61.59
Residual Error	2	0.9877			4.72
Total	8	20.9342			

Fig. 10 Contributions of key parameters (X, α, β, Error) on biosensor detection time

3.4.6 Analysis of Variance

The Analysis of Variance (ANOVA) is used to investigate which parameters significantly affected the quality characteristics and to estimate the percentage of key factors on the response time of the biosensor. In ANOVA many quantities as the degree of freedom (DoF), the sums of squares (SS), the F-ratio (F), and the percentage contribution are determined. Table 7 illustrates the ANOVA results for response time.

It is clear from Table 7 and Fig. 10 that the main contributions is related to the confinement coefficient β ($\sim$27%) and the confinement position X ($\sim$62%) while the angle of inclination (α) has the minimum contribution ($\sim$7%) to reduce response time among the key factors.

3.4.7 Prediction and verification

Under the optimal setting conditions, the optimal value of the microfluidic biosensor response time is estimated as follows:

$$\hat{T}_R = \overline{\beta}_3 + \overline{X}_2 - \overline{T}_R = 4.69 + 4.64 - 5.22 = 4.11 \text{ min} \tag{9}$$

where $\overline{\beta}_3$ is the average T_R for β at level 3 obtained from Table 6, $\overline{X}_2$ is the average T_R for X at level 2 obtained from Table 5, $\overline{T}_R$ is the mean of T_R. By running the FEM simulation under the optimal tuning conditions, we can get $T_R = 3.71$ min, relative error: $\left| \frac{T_R - \hat{T}_R}{T_R} \right| \times 100 = 10.66\%$, which is acceptable in engineering.

3.4.8 Comparison with experimental data

In Fig. 11, we plotted the completion time related to the work of Hofmann et al. [25] against that of our study to verify the validity of the confinement effect on the binding reaction in the biosensor. Our simulation appears to respond faster than Hofmann et al. [25], probably because the k_{on} and k_{off} values used in our study are higher than those of Cy5-labeled anti-rabbit IgG used by Hofmann et al. [25]. The response time found by Hofmann et al. [25] is higher than that obtained in our present work because the affinity of the Cy5-labeled rabbit anti-IgG molecule is higher than that used in our study.

Fig. 11 Comparison of the response time obtained by our work with that reported by Hofmann et al. [25]
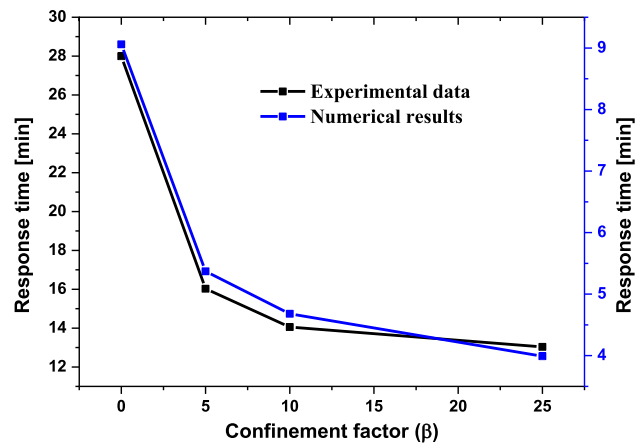
Fig. 12 Cross-correlation of predicted by MLR model and actual values of TR
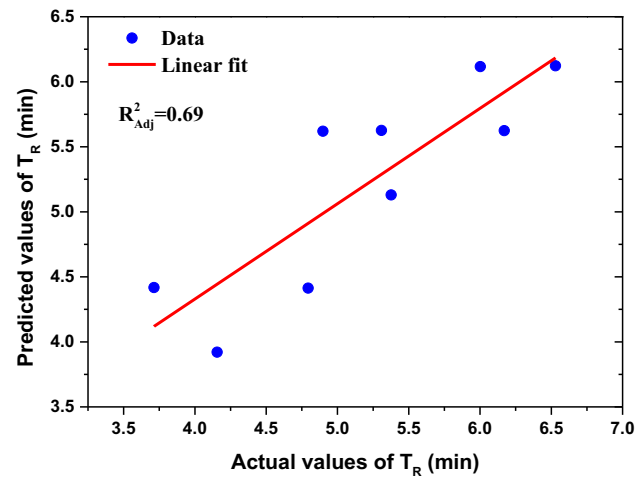
4 Predictive models

4.1 Modeling using Multiple linear regression analysis

Multiple linear regression (MLR) technique is employed to ascertain the relationship prevailing among the variables. In the multiple linear regression, the response Y takes the following form [15].

$$Y = a_0 + \sum_{i=1}^{N} a_i X_i \tag{10}$$

where $Y \equiv T_R$ is the response (the unit is minutes), a_0 is the average of response, X_i are the known variables on which predictions are to be made and a_i are the coefficients which are determined by the least squares method using the MATLAB software. In our case the multiple regression model gives:

$$T_R = 5.609 - 0.00789\boldsymbol{\alpha} - 0.0486\boldsymbol{\beta} + 0.01833X \tag{11}$$

The relationship between the numerical simulation values and those predicted by the multiple linear regression model for response time is shown in Fig. 12. Based on this figure, it can be seen that MLR data points are moderately dispersed around the regression line. The error in these two sets of values is due to the MLR model which does not take into account the interactions between the control factors: $\alpha\beta$, αX, βX, and $\alpha\beta X$.

The previous models are valid for $30° \leq \alpha \leq 90°$, $5 \leq \beta \leq 25$ and $0 \leq X \leq 80 \ \mu m$. A positive value in the models of Eq. 10 indicates a synergistic effect and a negative value indicates an opposite effect, and the absolute values of the coefficients indicate their significance for the response time.

Figure 13 illustrates the isosurfaces of response time as a function of principal key factors: Inclination angle α, confinement coefficient β and confinement position X. The revelant results prove that the model obtained with the multiple linear regression gives similar results as previous approaches.

Fig. 13 Surface plot for response time versus α, β and X. **a** TR = f(α, β), **b** TR = f(α, X), and **c** TR = f(β, X)
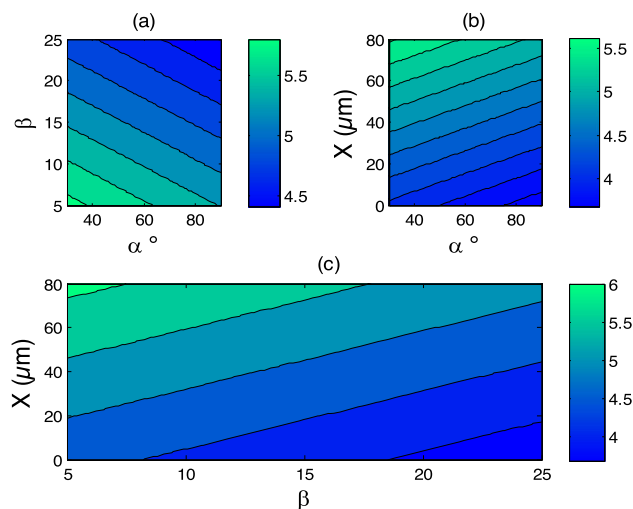
Fig. 14 ANN structure
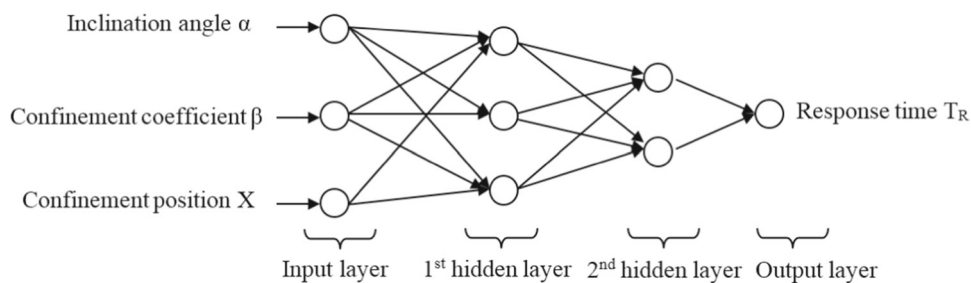
The design of experiment method shows that it is possible to optimize an efficient, inexpensive and reliable microfluidic biosensor in a very short period of time aimed at fighting against pandemics. These results prove the accuracy of this method compared to other previous numerical studies [29, 47]. The above numerical analysis by the design of experiment method shows the effects of optimization factors on analyte transport by concevtion-diffusion and binding kinetics. It allows us to determine the optimal position and inclination as well as the optimal confinement factor in a microfluidic biosensor for a better approach of the target molecules to the reaction surface by reducing or eliminating the diffusive boundary layer. Improving microfluidic biosensor performance by confining analytes with secondary flow is efficient and economical. The optimal detection time found by experimental design method shows that it is very small compared to other methods that use the electrothermal force [31, 48–50]. Based on this multiple linear regression model and using a genetic algorithm (GA) included in MATLAB software [51], the best combination giving the minimum response time in the studied intervals of these factors is the following: $\alpha = 90°$, $\beta = 25$, and $X = 40\ \mu m$.

According this combination, the response time obtained with the GA is $T_R = 3.6839$ min. In comparison with that obtained by the optimal combination obtained by the ANOVA analysis ($T_R = 3.71$ min) a reduction of 0.7% is achieved.

4.2 Modeling using artificial neural network (ANN)

An artificial neural network (ANN) is a system inspired by the functioning of biological neurons. It is then related to statistical methods and are generally optimized by probabilistic-type learning methods. The computed data, based on the OA design, is used to develop and train the ANN. The input and output parameters used to model the ANN are shown in Fig. 14.

The optimization of a number of hidden layer neurons is important in artificial intelligence. For this, several networks with different hidden layer neurons were trained and tested using the simulation data in Table 9. Figure 15 illustrates the mean absolute percentage error as a function of the number of neurons in the hidden layer. The network with the minimum error percentage (15 neurons in the hidden layer) was chosen as the optimal network (Fig. 15).

The model configuration used in this study is displayed in Table 8.

After learning the network, a test is assigned to predict the response time of the microfluidic biosensor to affirm the consistency of this model. The input data used to training the ANN are generated based on the ANOVA analysis using full factorial design. Table 9 and Fig. 16a present a comparison of the numerical simulation, the fitted data (ANOVA analysis), and the results predicted by the ANN. From these results, it can be observed that the response time of the biosensor predicted by the ANN model exhibits excellent consistency with the simulation data with an average percentage error lower to 1.5%.

A comparison of the results predicted by ANN model and simulation results of T_R is shown in Fig. 16. A regression coefficient very close to unity (R^2:0.98) is obtained (Fig. 16). From this figure, it can be seen that the points predicted by the ANN model are

Fig. 15 Mean percent error versus the hidden layer neuron number
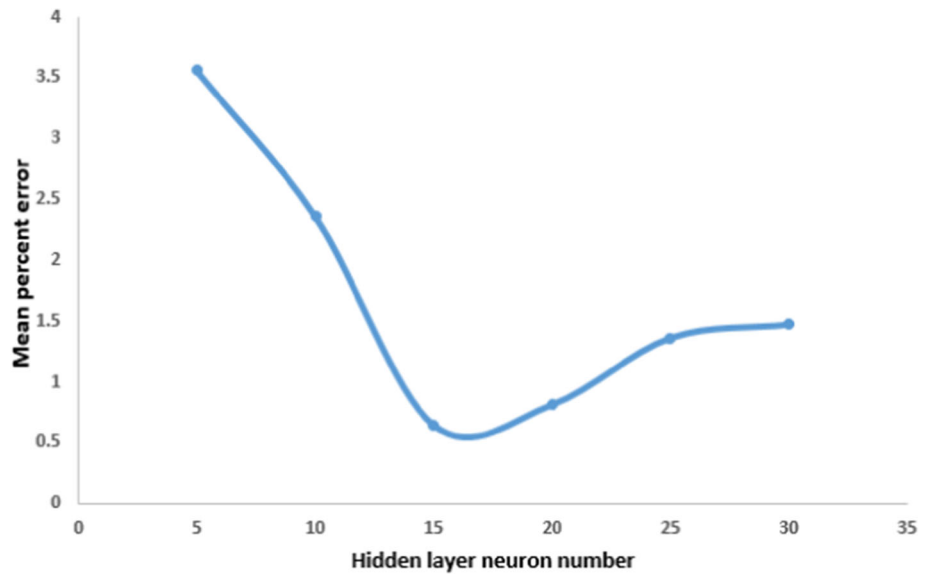
Table 8 Model configuration

Parameter	Description
Transfer function	Log sigmoid
Training	Levenberg–Marquardt
Network algorithm	Gradient descent (LEARNGD)
Performance function	Mean squared error

Table 9 Response time obtained by numerical simulation and predicted by ANN model

Experimental test	Factors			T_R (Exp)	T_R (ANN)	% Error
	A	B	C			
1	30	0.1	0	5.3769	5.3834	0.121
2	30	1.2	40	4.8983	4.8889	0.192
3	30	2.5	80	6.1701	6.1539	0.263
4	60	0.1	40	5.3088	5.0748	4.408
5	60	1.2	80	6.0022	6.0761	1.231
6	60	2.5	0	4.1563	4.0308	3.020
7	90	0.1	80	6.5292	6.547	0.273
8	90	1.2	0	4.7944	4.7836	0.225
9	90	2.5	40	3.7128	3.8522	3.755

Table 10 Performance indices (RMSE, VAF, MAPE, R^2, and R^2_{adj}) for models

Model	MAPE%	VAF (%)	RMSE (min)	R^2	R^2_{adj}
MLR	0.08	73.27	0.45	0.73	0.57
ANN	0.02	98.64	0.10	0.99	0.98

RMSE root-mean-square error, *MAPE* mean absolute percentage error

close to the regression line. The values of RMSE, VAF, and R^2 shown in Table 10 indicated that the ANN model showed the best prediction performance compared to MLR model.

According to Fig. 17, MSE gradients for the response time are shown as a function of the number of epochs during the training of the selected network. According to Fig. 17, the MSE gradients for the response time are plotted as a function of the number of epochs during the training of the selected network. From this figure, the best validation performance is obtained at epoch 20 where the gradient is 6.4353×10^{-5}.

Fig. 16 Cross-correlation of predicted and actual values of TR for ANN model
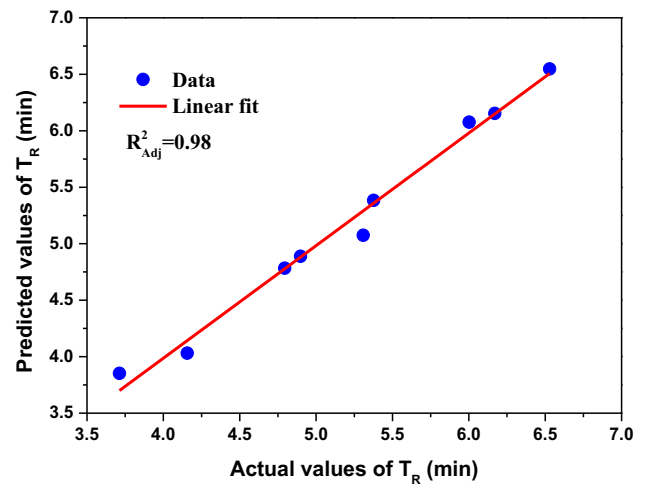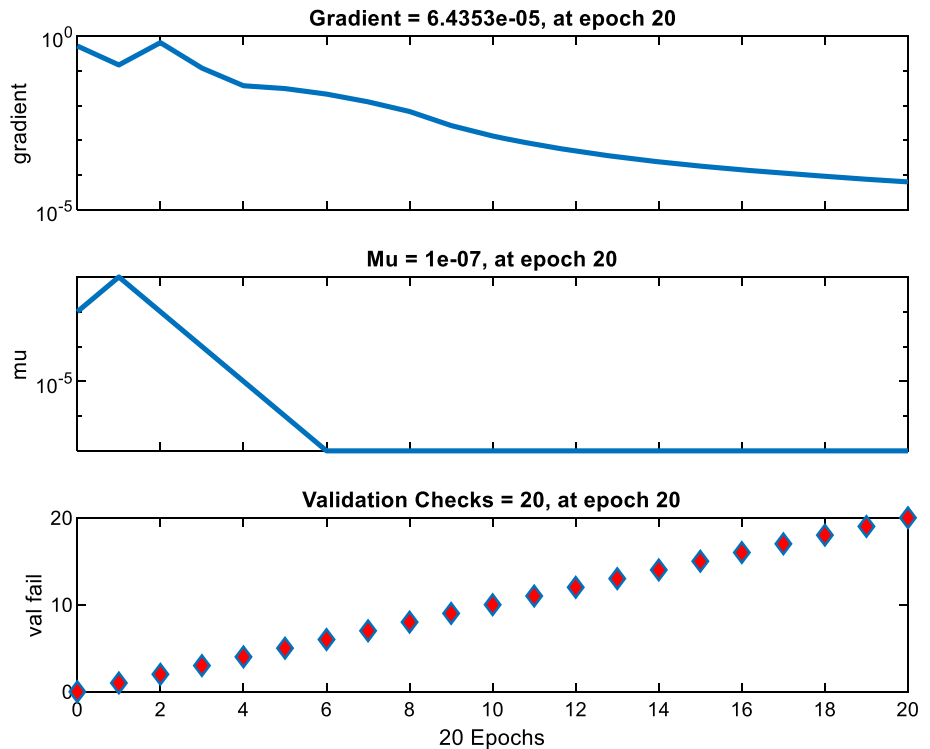

Fig. 17 Learning behavior of the ANN model

Figure 18 illustrates the regression between the network outputs and the corresponding targets during the training, the validation, and the testing process. The ideal model and the best match are respectively represented by a dotted line and a solid line. The output and the target are related by the value of R.

The efficient neural network chosen is one that regresses through training, validation, and testing with an R value very close to 1 (Fig. 18). The correlation coefficients (R) are 0.89 for training, 0.97 for validation, 0.999 for testing and 0.998 for the set in the simulation T_R. Therefore, this trained network can be used to predict responses for datasets used in microfluidic biosensor simulation.

4.3 Comparison between MLR and ANN predictive models

In order to evaluate the performance of the prediction capacity of the different model, the following coefficients are used [52, 53]:

- Value adjustment factor

$$\text{VAF} = \left[1 - \frac{\text{var}(y - \hat{y})}{\text{var}(y_i)} \right] \times 100 \tag{12}$$

Fig. 18 Linear regression analysis between the values calculated numerically with the finite element method and the predicted values ANN of the response time TR for the training, the validation, the tests and the assembly
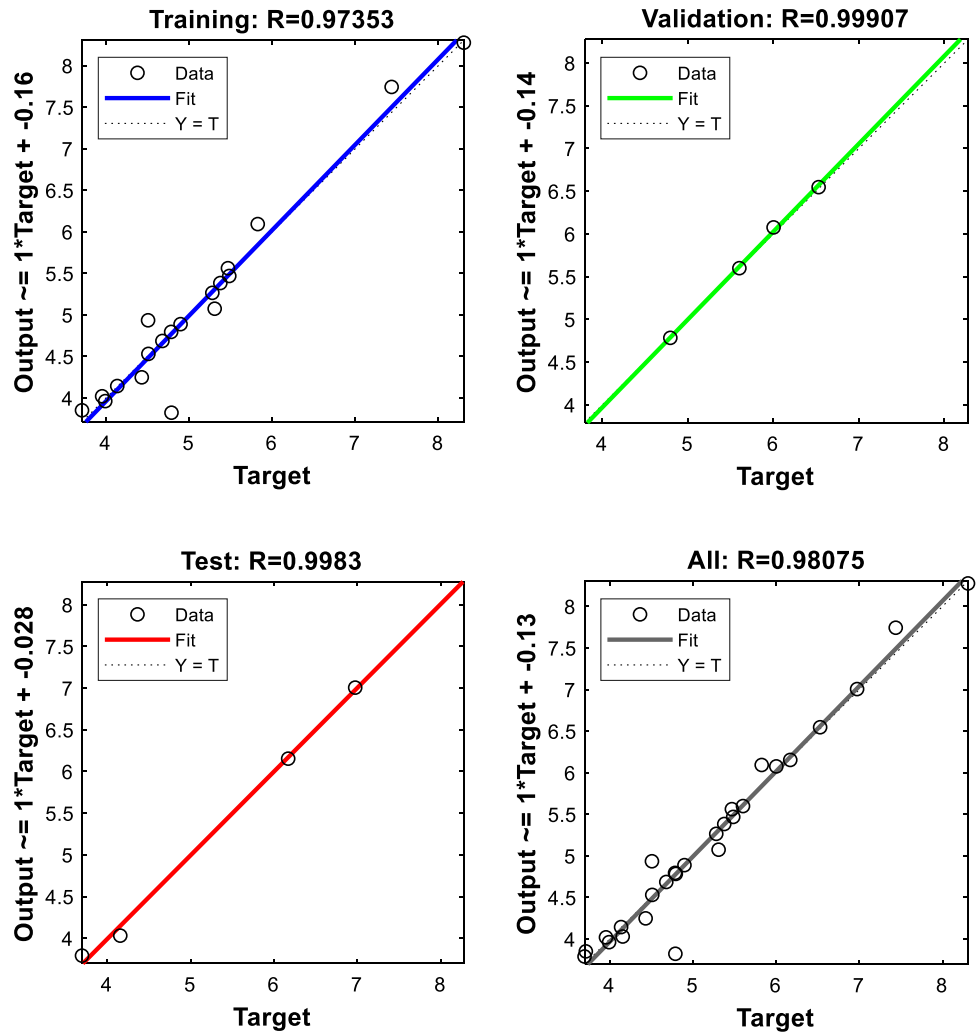
- Root-mean-square error

$$\mathrm{RMSE} = \sqrt{\frac{1}{N} \sum_{i=1}^{N} (y_i - \hat{y}_i)^2} \qquad (13)$$

- Mean absolute percentage error

$$\mathrm{MAPE} = \frac{1}{N} \sum_{i=1}^{N} \left| \frac{y_i - \hat{y}_i}{y_i} \right| \qquad (14)$$

- Correlation coefficient

$$R^2 = 1 - \frac{\sum_{i=1}^{N} (y_i - \hat{y}_i)^2}{\sum_{i=1}^{N} (\overline{y} - y_i)^2} \qquad (15)$$

- Adjusted R squared

$$R_{\mathrm{adj}}^2 = 1 - (1 - R^2) \times \frac{N - 1}{N - k - 1} \qquad (16)$$

where VAF is value adjustment factor, RMSE is root-mean-square error, MAPE is mean absolute percentage error, R^2 is the coefficient of determination, and R_{adj}^2 is the adjusted R^2. y_i is the actual value, $\hat{y}_i$ is the predicted value, $\overline{y}$ is average value of y, and k is number of input variables. When the value of VAF is 100 and RMSE is 0, then the model will be excellent. A large R^2 value (around 1) proves that the regression model fits the data well.
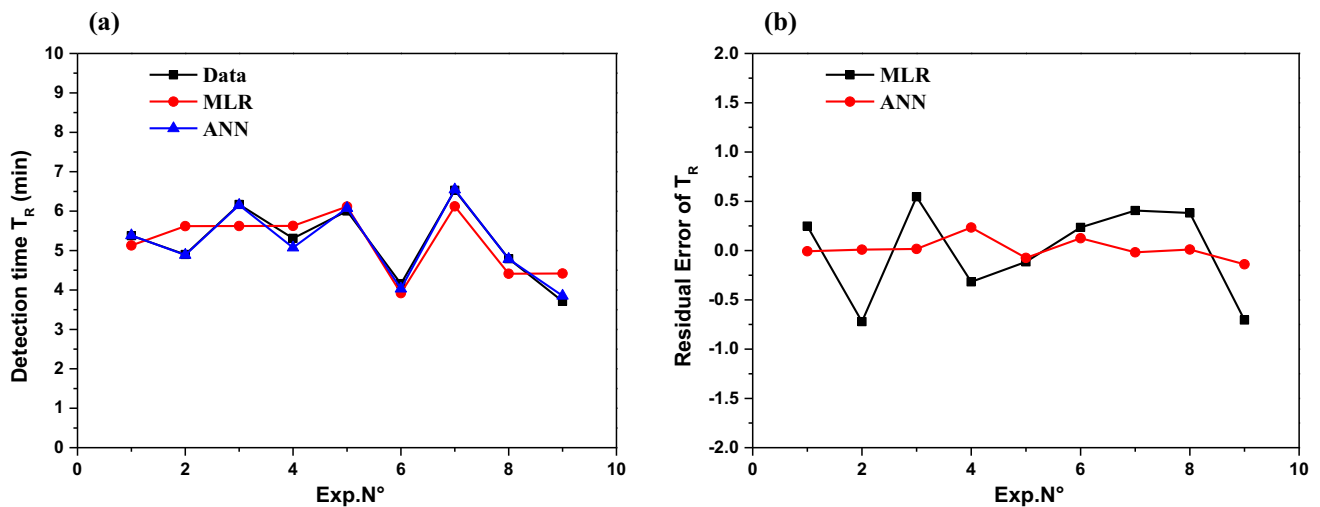
Fig. 19 **a** Simulation data and ANN data compared, and **b** the variation of the values predicted by ANN model from the CFD values

In this section, the results calculated by multiple linear regression (MLR) model, and ANN model in order to predict the response time of microfluidic biosensor were compared to the results calculated by finite element method. In order to evaluate the performance of the prediction capacity of these models, we calculate the quantities defined above, namely the value adjustment factor VAF, the root-mean-square error RMSE, the mean absolute percentage error MAPE, the correlation coefficient R^2, and adjusted value of R^2.

The comparative study of these models is illustrated in Fig. 19a and b. The MAPE, VAF, RMSE, R^2, and R^2_{adj} and the Taylor Diagram are used to show the most efficient and simple model to predict the response time of the microfluidic biosensor.

In Fig. 19b, the distances of the predicted values of the models built from the simulation values are shown to illustrate how far they depart from the observed values of T_R. This graph indicates that the deviation intervals (-0.72 min to $+0.55$ min) of the predicted values from ANN are smaller than the deviation intervals of MLR (-0.14 to $+0.23$ min).

The capabilities of the MLR and ANN models to predict the response time of microfluidic biosensor were examined by equating the responses of each approach to observed data, thereby calculating MAPE, VAF, RMSE, R^2, and R^2_{adj} using Eqs. (11)–(15), as shown in the Taylor diagram (Fig. 20) and Table 10. Developed by Karl E. Taylor [34], Taylor diagrams show which model is most realistic for a specific phenomenon. Three statistics are used here to measure the model's suitability—Pearson's correlation coefficient, root-mean-square error (RMSE), and standard deviation. It is demonstrated in Fig. 20 that only the predicted by the ANN model and the observed values of R^2, the standard deviation and the RMSE for the response time are statistically significant, whereas the MLR model is not statistically significant since $R^2 < 0.9$. Only the ANN model is taken into account for data prediction and optimization. The ANN model, indicated by point C, is closest to point A in terms of correlation coefficient R^2 and standard deviation. This indicates that the ANN model is the most realistic for prediction of microfluidic biosensor response time with confinement. Nevertheless, the values of R^2, R^2_{adj}, RMSE, MAE and VAF are much better for ANN than the MLR method (Table 10). The results illustrated in Figs. 12 and 16 show that the fluctuation distribution for ANN is much smaller and regular than that obtained by the MLR model. From Table 10; Figs. 12, 16 and 20, it can be concluded that ANN is superior to MLR.

5 Conclusion

The time detection of the virus plays a key role in fighting against the COVID-19 pandemic. Thus, the study of the response time of a biosensor seems to be crucial to saving lives and the economy. In this study, the best combination of microfluidic biosensor confinement parameters, namely confinement coefficient β, position of the confinement flow X and its inclination relative α to the main channel to minimize detection time was determined. Taguchi's approach, ANOVA analysis, multiple linear regression (MLR) model and predictive ANN model were used. Based on the results and analysis, the following conclusions can be drawn:

- An optimal combination of control parameters to minimize the detection time was obtained by using the S/N ratio. The optimal control factor settings obtained are shown as $\alpha = 90°$(level 3), $\beta = 25$ (level 3) and $X = 40\,\mu m$ (level 2) for minimum detection time.
- From the ANOVA analysis, X was found to be the most dominant parameter for response time with a percentage contribution of 62%.
- The R^2 values were calculated as 0.73 for the MLR model and 0.99 for the ANN model to predict the response time of this microfluidic biosensor.

Fig. 20 Taylor diagrams of the developed LMR and ANN models
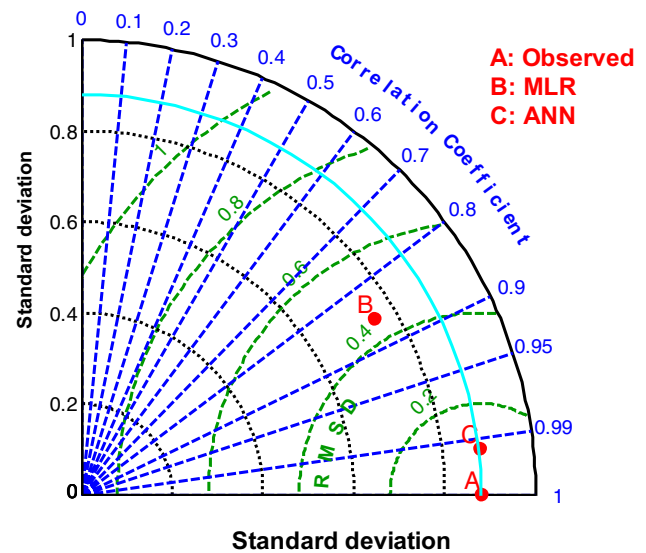
- The VAF values were calculated as 73.23% for the MLR model and 98.64% for the ANN model to predict the response time of this microfluidic biosensor.
- Based on R^2, and VAF the ANN model performed better than the MLR model in terms of prediction accuracy.

The design and optimization of an effective detection system, aiming to fight against the COVID-19 pandemics can be possible with an accurate numerical simulation which can be inexpensive and reliable in a short period of time.

Data Availability Statement This manuscript has associated data in a data repository [Authors' comment: The datasets generated during and/or analyzed during the current study are available from the corresponding author on reasonable request.].

Declarations

Conflict of interest The authors declare that they have no known competing financial interests or personal relationships that could have appeared to influence the work reported in this paper.

Human and animal rights The study does not involve humans or animals.

References

1. F. Shahbazi, M. Jabbari, M. N. Esfahani, and A. Keshmiri, Numerical simulation of Langmuir–Hinshelwood mechanism for heterogeneous biosensors in microfluidic channel. in *European Medical and Biological Engineering Conference* (Springer, 2020), pp. 905–914
2. C. Tymm, J. Zhou, A. Tadimety, A. Burklund, J.X. Zhang, Scalable COVID-19 detection enabled by lab-on-chip biosensors. Cell. Mol. Bioeng. **13**(4), 313–329 (2020)
3. P. Liu et al., A universal bonding method for preparation of microfluidic biosensor. Microfluid. Nanofluid. **25**(5), 1–10 (2021)
4. C. Huang et al., Clinical features of patients infected with 2019 novel coronavirus in Wuhan, China. Lancet **395**(10223), 497–506 (2020)
5. F. Shahbazi, M. Jabbari, M.N. Esfahani, A. Keshmiri, A computational simulation platform for designing real-time monitoring systems with application to COVID-19. Biosens. Bioelectron. **171**, 112716 (2021)
6. A. Parihar, P. Ranjan, S.K. Sanghi, A.K. Srivastava, R. Khan, Point-of-care biosensor-based diagnosis of COVID-19 holds promise to combat current and future pandemics. ACS Appl. Bio Mater. **3**(11), 7326–7343 (2020)
7. R.A. Escalona-Villalpando, A. Sandoval-García, M. Miranda-Silva, L. Arriaga, S.D. Minteer, J. Ledesma-García, A self-powered glucose biosensor device based on microfluidics using human blood. J. Power Sources **515**, 230631 (2021)
8. W.-C. Tai, Y.-C. Chang, D. Chou, L.-M. Fu, Lab-on-paper devices for diagnosis of human diseases using urine samples—a review. Biosensors **11**(8), 260 (2021)
9. T. Dong, N.M.M. Pires, Immunodetection of salivary biomarkers by an optical microfluidic biosensor with polyethylenimine-modified polythiophene-C70 organic photodetectors. Biosens. Bioelectron. **94**, 321–327 (2017)
10. Z. Kotsiri, J. Vidic, A. Vantarakis, Applications of biosensors for bacteria and virus detection in food and water–a systematic review. J Environ Sci **111**, 367–379 (2022)
11. Y. Song et al., Recent progress in microfluidics-based biosensing. Anal. Chem. **91**(1), 388–404 (2018)

12. Y. Cao, B. Zhang, Z. Zhu, X. Xin, H. Wu, B. Chen, Microfluidic based whole-cell biosensors for simultaneously on-site monitoring of multiple environmental contaminants. Front. Bioeng. Biotechnol. **9**, 622108 (2021)

13. A. Nilghaz, S.M. Mousavi, M. Li, J. Tian, R. Cao, X. Wang, based microfluidics for food safety and quality analysis. Trends Food Sci. Technol. **118**, 273–284 (2021)

14. X. Wang, Y. Xie, L. Lin, Recent development of microfluidic biosensors for the analysis of antibiotic residues. TrAC Trends Anal. Chem. **157**, 116797 (2022)

15. J.R. Choi, Development of point-of-care biosensors for COVID-19. Front. Chem. **8**, 517 (2020)

16. N. Farshidfar, S. Hamedani, The potential role of smartphone-based microfluidic systems for rapid detection of COVID-19 using saliva specimen. Mol. Diagn. Ther. **24**(4), 371–373 (2020)

17. G. Seo et al., Rapid detection of COVID-19 causative virus (SARS-CoV-2) in human nasopharyngeal swab specimens using field-effect transistor-based biosensor. ACS Nano **14**(4), 5135–5142 (2020)

18. L.A. Layqah, S. Eissa, An electrochemical immunosensor for the corona virus associated with the Middle East respiratory syndrome using an array of gold nanoparticle-modified carbon electrodes. Microchim. Acta **186**(4), 1–10 (2019)

19. M. Javanmard, A.H. Talasaz, M. Nemat-Gorgani, F. Pease, M. Ronaghi, R.W. Davis, Electrical detection of protein biomarkers using bioactivated microfluidic channels. Lab Chip **9**(10), 1429–1434 (2009)

20. H. Dong, C.-M. Li, Y.-F. Zhang, X.-D. Cao, Y. Gan, Screen-printed microfluidic device for electrochemical immunoassay. Lab Chip **7**(12), 1752–1758 (2007)

21. C.D. Chin et al., Microfluidics-based diagnostics of infectious diseases in the developing world. Nat. Med. **17**(8), 1015–1019 (2011)

22. L. Lafleur et al., Progress toward multiplexed sample-to-result detection in low resource settings using microfluidic immunoassay cards. Lab Chip **12**(6), 1119–1127 (2012)

23. Y.-F. Lee, K.-Y. Lien, H.-Y. Lei, G.-B. Lee, An integrated microfluidic system for rapid diagnosis of dengue virus infection. Biosens. Bioelectron. **25**(4), 745–752 (2009)

24. D.B. Hibbert, J.J. Gooding, P. Erokhin, Kinetics of irreversible adsorption with diffusion: application to biomolecule immobilization. Langmuir **18**(5), 1770–1776 (2002)

25. O. Hofmann, G. Voirin, P. Niedermann, A. Manz, Three-dimensional microfluidic confinement for efficient sample delivery to biosensor surfaces. Application to immunoassays on planar optical waveguides. Anal. Chem. **74**(20), 5243–5250 (2002)

26. M. Abrantes, M.T. Magone, L.F. Boyd, P. Schuck, Adaptation of a surface plasmon resonance biosensor with microfluidics for use with small sample volumes and long contact times. Anal. Chem. **73**(13), 2828–2835 (2001)

27. M. Selmi, R. Khemiri, F. Echouchene, H. Belmabrouk, Electrothermal effect on the immunoassay in a microchannel of a biosensor with asymmetrical interdigitated electrodes. Appl. Therm. Eng. **105**, 77–84 (2016)

28. M. Selmi, F. Echouchene, H. Belmabrouk, Analysis of microfluidic biosensor efficiency using a cylindrical obstacle. Sens. Lett. **14**(1), 26–31 (2016)

29. M. Selmi, F. Echouchene, M.H. Gazzah, H. Belmabrouk, Flow confinement enhancement of heterogeneous immunoassays in microfluidics. IEEE Sens. J. **15**(12), 7321–7328 (2015)

30. F. Echouchene, T. Al-shahrani, H. Belmabrouk, Enhancement of heterogeneous microfluidic immunosensors using new sensing area shape with electrothermal effect. Appl. Sci. **11**(10), 4566 (2021)

31. S. Kaziz, Y. Saad, M.H. Gazzah, H. Belmabrouk, 3D simulation of microfluidic biosensor for SARS-CoV-2 S protein binding kinetics using new reaction surface design. Eur. Phys. J. Plus **137**(2), 1–12 (2022)

32. S. Kaziz, I. Ben Mariem, F. Echouchene, M. Belkhiria, H. Belmabrouk, Taguchi optimization of integrated flow microfluidic biosensor for COVID-19 detection. Eur. Phys. J. Plus **137**(11), 1–12 (2022)

33. S. Kaziz, I.B. Romdhane, F. Echouchene, M.H. Gazzah, Numerical simulation and optimization of AC electrothermal microfluidic biosensor for COVID-19 detection through Taguchi method and artificial network. Eur. Phys. J. Plus **138**(1), 96 (2023)

34. I. Ben Mariem, S. Kaziz, M. Belkhiria, F. Echouchene, H. Belmabrouk, Numerical optimization of microfluidic biosensor detection time for the SARS-CoV-2 using the Taguchi method. Indian J. Phys. (2023). https://doi.org/10.1007/s12648-023-02632-z

35. S. Kaziz, I. Ben Mariem, F. Echouchene, M.H. Gazzah, H. Belmabrouk, Design parameters optimization of an electrothermal flow biosensor for the SARS-CoV-2 S protein immunoassay. Indian J. Phys. (2022). https://doi.org/10.1007/s12648-022-02360-w

36. M. Selmi, R. Khemiri, F. Echouchene, H. Belmabrouk, Enhancement of the analyte mass transport in a microfluidic biosensor by deformation of fluid flow and electrothermal force. J. Manuf. Sci. Eng. **138**(8), 081011 (2016)

37. F. Echouchene, T. Al-Shahrani, H. Belmabrouk, Simulation of the slip velocity effect in an AC electrothermal micropump. Micromachines **11**(9), 825 (2020)

38. P.R. Aranda, G.A. Messina, F.A. Bertolino, S.V. Pereira, M.A.F. Baldo, J. Raba, Nanomaterials in fluorescent laser-based immunosensors: Review and applications. Microchem. J. **141**, 308–323 (2018)

39. A. Bange, H.B. Halsall, W.R. Heineman, Microfluidic immunosensor systems. Biosens. Bioelectron. **20**(12), 2488–2503 (2005)

40. H. Filik, A.A. Avan, Electrochemical immunosensors for the detection of cytokine tumor necrosis factor alpha: a review. Talanta **211**, 120758 (2020)

41. S. Jeong, M.-J. Park, W. Song, H.-S. Kim, Current immunoassay methods and their applications to clinically used biomarkers of breast cancer. Clin. Biochem. **78**, 43–57 (2020)

42. F. Echouchene, T. Al-Shahrani, H. Belmabrouk, Analysis of temperature-jump boundary conditions on heat transfer for heterogeneous microfluidic immunosensors. Sensors **21**(10), 3502 (2021)

43. V. Levich, N. Amundson, *Motion and diffusion in thin liquid films* (Prentice-Hall, Englewood Cliffs, 1962), pp.669–700

44. S. Brooks, I. Higgins, J. Newman, A. Turner, Biosensors for process control. Enzyme Microb. Technol. **13**(12), 946–955 (1991)

45. C. Qi et al., Investigation of interaction between two neutralizing monoclonal antibodies and SARS virus using biosensor based on imaging ellipsometry. Biomed. Microdevice **8**(3), 247–253 (2006)

46. R. Nath, M. Krishnan, Optimization of double diffusive mixed convection in a BFS channel filled with alumina nanoparticle using Taguchi method and utility concept. Sci. Rep. **9**(1), 19536 (2019)

47. C.-K. Yang, J.-S. Chang, S.D. Chao, K.-C. Wu, Two dimensional simulation on immunoassay for a biosensor with applying electrothermal effect. Appl. Phys. Lett. **91**(11), 113904 (2007)

48. K.-R. Huang, J.-S. Chang, Three dimensional simulation on binding efficiency of immunoassay for a biosensor with applying electrothermal effect. Heat Mass Transf. **49**(11), 1647–1658 (2013)

49. K.-R. Huang et al., Simulation on binding efficiency of immunoassay for a biosensor with applying electrothermal effect. J. Appl. Phys. **104**(6), 064702 (2008)

50. S. Kaziz, Y. Saad, M. Bouzid, M. Selmi, H. Belmabrouk, Enhancement of COVID-19 detection time by means of electrothermal force. Microfluid. Nanofluid. **25**(10), 1–12 (2021)

51. S. Samanta, Genetic algorithm: an approach for optimization (Using MATLAB). Int. J. Latest Trends Eng. Technol. (IJLTET) **3**(3), 261–267 (2014)
52. S. Amid, T. Mesri Gundoshmian, Prediction of output energies for broiler production using linear regression, ANN (MLP, RBF), and ANFIS models. Environ. Prog. Sustain. Energy **36**(2), 577–585 (2017)
53. S. Tayyebi, Z. Hajjar, S. Soltanali, A novel modified training of radial basis network: prediction of conversion and selectivity in 1-hexene dimerization process. Chemom. Intell. Lab. Syst. **190**, 1–9 (2019)